Journal of Medicinal Chemistry Article

J. Med. Chem. **2010,** *53,* 4633–4641 **4633**
DOI: 10.1021/jm1001293

Evaluation of Re and ^{99m}Tc Complexes of 2-(4′-Aminophenyl)benzothiazole as Potential Breast Cancer Radiopharmaceuticals

Stamatia Tzanopoulou,[†] Marina Sagnou,[†] Maria Paravatou-Petsotas,[‡] Eleni Gourni,[‡] George Loudos,[§] Stavros Xanthopoulos,[‡] Daniel Lafkas,[∥] Hippokratis Kiaris,[∥] Alexandra Varvarigou,[‡] Ioannis C. Pirmettis,[‡] Minas Papadopoulos,[‡] and Maria Pelecanou*[,†]

[†]*Institute of Biology, and* [‡]*Institute of Radioisotopes-Radiodiagnostic Products, National Centre for Scientific Research "Demokritos", 15310 Athens, Greece,* [§]*Department of Medical Instruments Technology, Technological Educational Institute of Athens, 12210 Athens, Greece, and* [∥]*Department of Biological Chemistry, University of Athens Medical School, 75 M. Asias Street, 11527 Athens, Greece*

Received January 31, 2010

The synthesis of M(I)(CO)$_3$(NNO) (M = Re, ^{99m}Tc) complexes conjugated to the antitumor agent 2-(4′-aminophenyl)benzothiazole and to its 6-methyl derivative, as well as their in vitro and in vivo biological evaluation as breast cancer radiopharmaceuticals, is reported. The Re complexes displayed under the fluorescence microscope clear uptake by the sensitive to the 2-(4′-aminophenyl)benzothiazole pharmacophore breast cancer cell lines MCF-7 and T47D, while uptake by less sensitive lines and by normal fibroblasts was much weaker. In accordance, uptake of the corresponding radioactive ^{99m}Tc complexes was clearly higher in the breast cancer cell lines MCF-7 and MDA-231 compared to normal fibroblasts. Biodistribution of the ^{99m}Tc complexes in SCID mice bearing MCF-7 xenografts showed appreciable tumor uptake. A tumor/muscle ratio of 2.2 was measured for the complex conjugated to 2-(4′-aminophenyl)benzothiazole that led to successful tumor imaging. The results render the 2-(4′-aminophenyl)benzothiazole complexes potential candidates for imaging (^{99m}Tc) and targeted radiotherapy (^{188}Re) of breast cancer.

Introduction

Members of the 2-(4′-aminophenyl)benzothiazole class (Figure 1A) possess highly selective, potent antitumor properties in vitro and in vivo.[1,2] The original lead compound in this series, 2-(4′-aminophenyl)benzothiazole (**1**), exhibits nanomolar in vitro activity against certain human breast cancer cell lines with a characteristic biphasic dose−response relationship.[3] Its discovery in 1996 was followed by the synthesis and evaluation of a series of substituted analogues with more potent and diverse activity and the identification of the 2-(4′-amino-3′-methylphenyl)benzothiazole (DF 203)[1,4] as the lead compound in this series on the basis of superior in vivo performance.[5−7] The result of this chemistry-driven approach to drug discovery encompassing synthesis, in vitro and in vivo biological evaluation, and mechanistic studies culminated in the development of the novel clinical candidate 2-(4′-amino-3′-methylphenyl)-5-fluorobenzothiazole lysylamide prodrug (Phortress, Figure 1B),[2] which is in phase I clinical trial in the U.K.[2,8]

The specificity of the action of the 2-(4′-aminophenyl)-benzothiazoles that are taken up and metabolized only by sensitive cancer cell lines with negligible uptake by unresponsive cell lines[1−8] makes this class of compounds ideal pharmacophores for the development of tumor-specific radiopharmaceuticals, serving as vehicles that carry the radionuclide of choice to the diseased tissue for diagnostic or therapeutic applications.[9] In a previous communication[10] we have reported the synthesis and initial biological evaluation of rhenium ($^{185/187}$Re) and technetium-99m (^{99m}Tc) complexes of

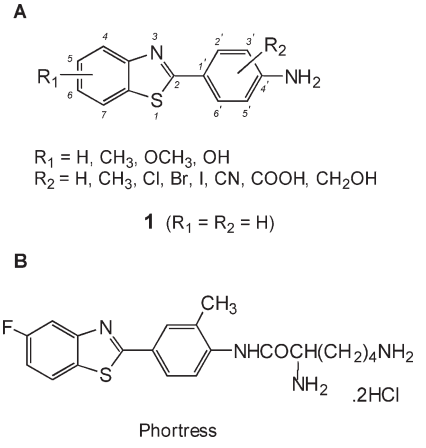

Figure 1. Chemical structures of (A) the antitumor 2-(4′-aminophenyl)benzothiazoles (**1** being the original lead compound in the series) and (B) the clinical candidate phortress.

2-(4′-aminophenyl)benzothiazole of the general formula M(I)-(CO)$_3$(NNO) (M = Re, ^{99m}Tc) (**2a** and **2b**, respectively, Figure 2) for breast cancer imaging and targeted radiotherapy. ^{99m}Tc (monoenergetic γ photons of 140 keV, $t_{1/2}$ of 6 h, lack of particulate emission) is widely used in clinical diagnostic imaging, while Re, the group VIIB congener of Tc, has two β-emitting isotopes suitable for therapeutic applications, ^{186}Re ($t_{1/2}$ = 3.8 d, E_{max} = 1.07 MeV) and ^{188}Re ($t_{1/2}$ = 0.7 d, E_{max} = 2.12 MeV).[11] Tc and Re form analogous complexes with very similar physical and chemical properties that are expected to have the same pharmacokinetic behavior and are therefore considered a "matched pair" for diagnosis and therapy.[12]

*To whom correspondence should be addressed. Phone: + 30 210 6503555. Fax: + 30 210 6511767. E-mail: pelmar@bio.demokritos.gr.

Published on Web 06/02/2010

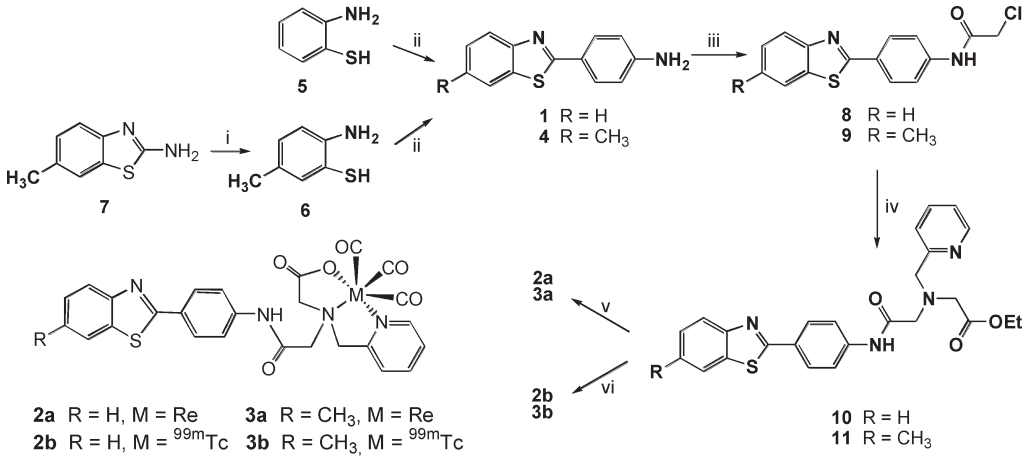

Figure 2. Synthesis of the target rhenium (**2a**, **3a**) and technetium (**2b**, **3b**) complexes: (i) NaOH (10 M), reflux o/n; (ii) PPA, 220 °C, 4 h; (iii) chloroacetyl chloride, triethylamine, dry CH_2Cl_2, 0 °C to room temp; (iv) PAMA, Hunig's base; (v) NaOH, $[NEt_4]_2[fac\text{-}Re(CO)_3(Br)_3]$, CH_3CN/H_2O, 70 °C; *fac*-$[^{99m}Tc(CO)_3(H_2O)_3]^+$, 75 °C.

We present herein the synthesis of complexes **3a** and **3b**, 6-methyl derivatives of complexes **2a** and **2b** respectively (Figure 2), the further in vitro evaluation of complexes **2a**, **2b**, **3a**, and **3b**, and the in vivo application of the ^{99m}Tc complexes **2b** and **3b** in MCF-7[a] tumor bearing SCID mice that establishes the potential of these labeled 2-(4′-aminophenyl)benzothiazole derivatives for radiopharmaceutical applications.

Results

Synthesis of Re and Tc Complexes. The target complexes **2** and **3** were efficiently prepared according to the synthetic scheme[10] presented in Figure 2. Briefly, the 2-(4′-aminophenyl)-benzothiazoles **1** and **4** were synthesized via polyphosphoric acid mediated oxidative condensation of 2-aminothiophenol (**5**) and 2-amino-5-methylthiophenol (**6**), respectively, with 4-aminobenzoic acid.[13,5] Compound **6** is not commercially available, and it was obtained by basic hydrolysis of 2-amino-6-methylbenzothiazole (**7**).[14] The aniline moiety of **1** and **4** was subsequently acetylated with chloroacetyl chloride in the presence of triethylamine to produce the halides **8** and **9** that further underwent nucleophilic substitution by the secondary amine of the *N*-(2-pyridylmethyl)aminoacetic acid ethyl ester (PAMA)[15] chelating moiety to yield ligands **10** and **11**.

Ligands **10** and **11** were successfully converted to the desired Re complexes **2a** and **3a** in high yield by ligand exchange reaction employing the organometallic Re tricarbonyl $[NEt_4]_2[fac\text{-}Re(CO)_3(Br)_3]$ precursor.[16] Basic hydrolysis of the ligand ester group took place in situ prior to the addition of the Re precursor. The complexes were crystallized from methanol and were fully characterized by elemental analyses and spectroscopic techniques.

The corresponding ^{99m}Tc complexes **2b** and **3b** were prepared at tracer level by ligand exchange reaction employing the *fac*-$[^{99m}Tc(CO)_3(H_2O)_3]^+$ precursor,[17] as previously described.[10] Prior basic hydrolysis of the ester group of ligands **10** and **11** was not necessary in this case. Apparently, the weak Lewis base character of technetium is sufficient to drive the complexation reaction forward with concomitant hydrolysis of the ester functionality of the ligands.[17] For both complexes the radiochemical yield was >95%.

The stability of both rhenium and technetium complexes was assessed under a variety of conditions. ^{99m}Tc complexes were stable for a period of at least 4 half-lives at room temperature in their preparation reaction mixture and in cell culture medium, as well as in the presence of histidine and cysteine.[10] Furthermore, Re complexes remained intact in human serum and in cell culture medium in the absence and presence of cells (Supporting Information).

Cell Uptake of Re Complexes by Cancer Lines. Cell uptake of the Re complexes and their ligands was monitored by fluorescence microscopy, taking advantage of the fluorescence properties of the 2-(4′-aminophenyl)benzothiazole unit. Microscope images from the uptake experiments of complexes **2a**, **3a**, and their corresponding ligands **10** and **11** in the MCF-7, MDA-231, and MDA-468 cancer cell lines and in HFFF-2 normal fibroblasts are shown in Figure 3. It can be clearly seen that the best uptake for **2a** and **10** is observed in the MCF-7 cell line, while **3a** and **11** give stronger signal in the MDA-231 cell line. Direct comparison of the degree of uptake of the complexes **2a** and **3a** in each cell line is not possible because the fluorescence of **2a** is much more intense than that of **3a** (Figure S2 in Supporting Information). The uptake of **2a** and **3a** by normal HFFF-2 fibroblasts was similar to that of untreated controls, indicating that uptake, if present, is quite low to give detectable fluorescence signal.

The uptake of complex **2a**, which clearly has the best properties for evaluation with fluorescence microscopy, was further examined in the T47D and SKBR-3 breast cancer cell lines, in the PC3 prostate cancer cell line, and in the MRC-5, MILA, and 3T3 normal fibroblast lines, and the

[a] Abbreviations: MCF-7, T47D, MDA-231, MDA-468, SKBR-3, breast cancer cell lines of human origin; PC3, prostate cancer cell line of human origin; 3T3, MRC-5, MILA, HFFF-2, normal fibroblast cell lines; SCID, severe combined immunodeficient; PAMA, *N*-(2-pyridylmethyl)aminoacetic acid; MTT, 3-(4,5-dimethythiazol-2-yl)-2,5-diphenyltetrazolium bromide; HPLC, high-performance liquid chromatography; AhR, aryl hydrocarbon receptor; CYP1A1, cytochrome P450, family 1, subfamily A, polypeptide 1; ROI, regions of interest; TFA, trifluoroacetic acid; FT-IR, Fourier transform infrared; ESI, electrospray ionization; UV/vis, ultraviolet/visible; COSY, correlation spectroscopy; HSQC, heteronuclear single quantum correlation; HMBC, heteronuclear multiple bond correlation; NOESY, nuclear Overhauser effect spectroscopy; DMSO, dimethyl sulfoxide; TMS, tetramethylsilane; DMEM, Dulbecco's modified Eagle medium; NMR, nuclear magnetic resonance; ID, injected dose; SPECT, single photon emission computerized tomography; p.i., post injection; PPD, *p*-phenylenediamine; EDTA, ethylenediaminetetraacetic acid; NIH, National Institutes of Health (U.S.); PBS, phosphate buffered saline; SPECT, single photon emission computed tomography.

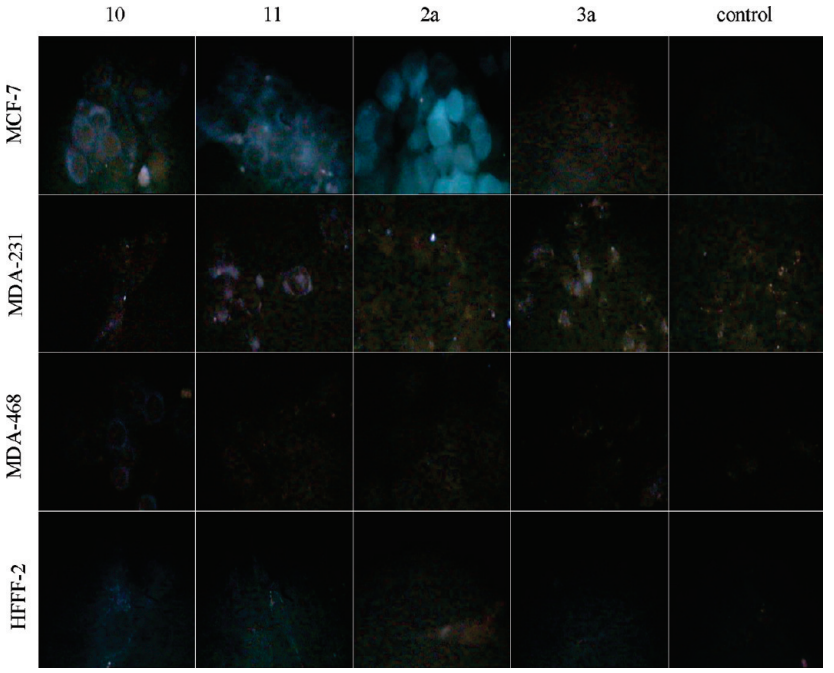

Figure 3. Evaluation of cell uptake based on fluorescence microscopy. Sensitive breast cancer cells MCF-7 and MDA-231, insensitive breast cancer cells MDA-468, and normal fibroblasts HFFF-2 were all incubated with 80 μM ligand **10**, ligand **11**, complex **2a**, or complex **3a** for 24 h. The cell fluorescence was observed using a D-F-T triple band filter (100×).

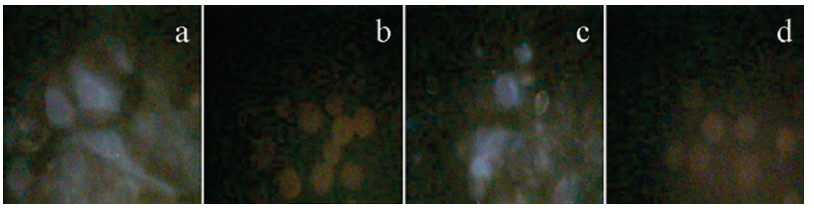

Figure 4. Microscopic observation of MCF-7 intact cells after 24 h (a) and 48 h (c) of incubation with complex **2a** (80 μM) and of their isolated nuclei (b, d). The nuclei showed no observable fluorescence.

results are shown in Figure S3. Weak uptake can be observed in T47D cells, while uptake by the SKBR-3 cells and all normal fibroblasts is not observable under the experimental conditions. The effect of concentration of **2a** on its uptake by MCF-7, T47D, and SKBR-3 cells is given in Figure S4 showing lower fluorescence signal at lower concentrations.

Cytotoxicity of Re Complexes in the MCF-7 Cell Line. The cytotoxic properties of complexes **2a** and **3a** were evaluated in the MCF-7 cell line by means of the MTT assay, and the corresponding cell viability curves are presented in Figure S5. Very low viability values were not reached because of the limited solubility of the complexes in aqueous medium that did not allow the employment of concentrations higher than 100 μM. When the existing data were fit to a sigmoidal curve with the PRISM program, a low limit for the IC_{50} is approximated at 800 nM for **2a** (IC_{50} > 800 nM for **2a**) and at 600 nM for **3a** (IC_{50} > 600 nM for **3a**). These values are approximately 2 orders of magnitude higher than the IC_{50} of < 10 nM reported in the MTT assay for the parent compound **1**[5,3] and approximately 1 order of magnitude higher than the IC_{50} < 100 nM reported for the acetylamide of **1**,[5] indicating the lower cytotoxicity of complexes **2a** and **3a** compared to the parent pharmacophores.

Nuclear Uptake Study of Re Complex 2a. In all cell uptake experiments the cell nuclei appear distinctly darker than the cytoplasm (Figure 3), suggesting the absence of the fluorescent complexes. To better examine the fluorescent properties of the nuclei and allow for a safer conclusion on the presence of **2a** in them, the preparation of an enriched nuclei sample was attempted. Specifically, after incubation of the MCF-7 cells with complex **2a** for 24 h according to the standard procedure, the cells were treated with a hypotonic solution of KCl, which gently removes the cytoplasm without interrupting the nucleus membrane, in order to enrich the sample in cell nuclei. The fluorescence images of the nuclei are shown in Figure 4, where it is obvious that no signal can be detected. In accordance with the fluorescence microscope observations, examination with confocal microscopy of MCF-7 cells after incubation with 80 μM **2a** reveals localization of **2a** within the cytoplasm while the nuclei appear as black areas with no visible presence of **2a** (Figure 5).

Cell Uptake of ^{99m}Tc Complexes 2b and 3b. The ability of the radioactive ^{99m}Tc complexes **2b** and **3b** to enter breast cancer cells was tested using the MCF-7 and MDA-231 cancer cell lines. As presented in Figure 6, at 5 h the percent of total radioactivity present in the cells ranges from 2.0 to 3.6. The radioactivity measured at all times in cancer cells is more than double the radioactivity observed in normal 3T3 fibroblasts serving as control. The difference in uptake by the MCF-7 cells between the Re complex **2a** and its 6-methyl analogue **3a** (Figure 3) (attributed mainly to the difference in their fluorescence properties) was not observed with the

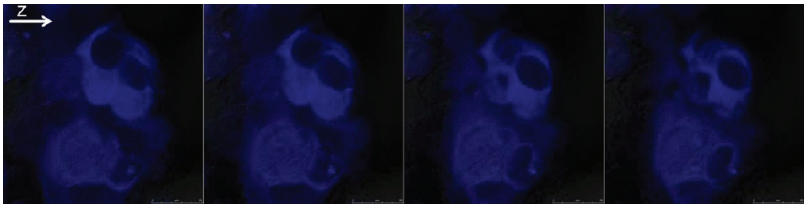

Figure 5. Consecutive (along the *z* axis) confocal microscopy photographs of MCF-7 cells after 24 h of incubation with 80 μM **2a**, using DAPI filter.

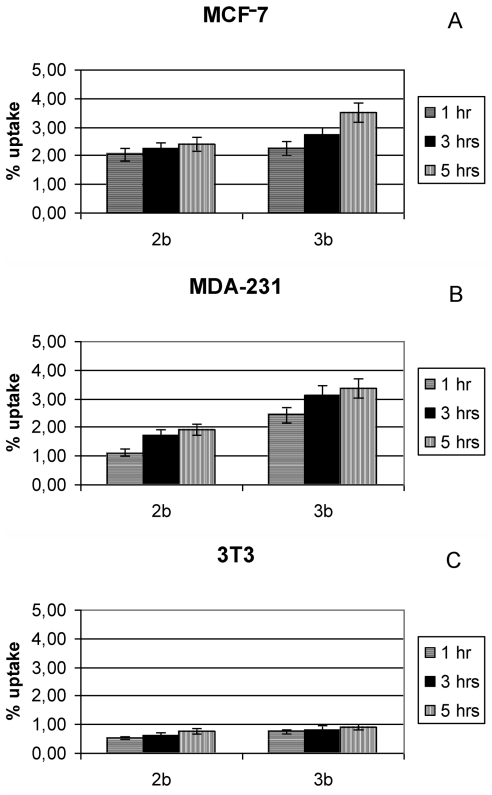

Figure 6. Radioactivity (expressed as percent of total radioactivity added) measured after incubation of (A) MCF-7 cancer cells, (B) MDA-231 cancer cells, and (C) 3T3 normal fibroblasts with the radioactive ^{99m}Tc complexes **2b** and **3b** for 1, 3, and 5 h.

^{99m}Tc analogues that gave comparable uptake results. In addition, the difference in uptake witnessed for the Re complex **2a** between the MCF-7 and MDA-231 cancer cells (Figure 3) was not observed with the ^{99m}Tc analogue **2b**. However, it is taken into account that the incubation with **2a** lasted for 24 h and at 5 h no uptake was visible for the MCF-7 cells as well. Attempting to increase the incubation time of **2b** to 24 h (with concomitant increase of the radioactivity employed to 1 μCi to take into account the decay of technetium) led to cell death, possibly due to radiolysis under the specific conditions. Observation with fluorescent microscope revealed dead cells and cells with altered morphology even at 18 h, making it impossible to pursue uptake studies with ^{99m}Tc at the length of time employed for the Re complexes.

Biodistribution in Mice Bearing MCF-7 Xenografts. The biodistribution data of complex **2b** in SCID mice bearing MCF-7 xenografts are presented in Table 1 as %ID/g for the 15 and 60 min p.i. time intervals. As expected from the biodistribution studies of the same complex in healthy mice,[10] complex **2b** is efficiently cleared from soft tissue

Table 1. Biodistribution of **2b** in MCF-7 Tumor-Bearing SCID Mice[a]

organ/tissue	15 min	60 min
blood	1.36 ± 0.24	0.62 ± 0.11
liver	20.27 ± 6.69	8.97 ± 0.13
heart	0.92 ± 0.26	0.83 ± 0.06
kidneys	14.63 ± 5.59	6.14 ± 1.15
stomach	3.60 ± 1.58	3.54 ± 0.07
intestines	15.17 ± 2.22	24.35 ± 0.77
spleen	1.28 ± 0.77	1.12 ± 0.22
muscle	0.48 ± 0.06	0.38 ± 0.06
lungs	1.82 ± 0.53	1.05 ± 0.06
tumour	1.04 ± 0.14	0.67 ± 0.06
tumor/blood	0.76	1.09
tumor/muscle	2.17	1.76

[a] Data are expressed as %ID/g tissue and are presented as the mean (n = 5) at 15 and 60 min p.i.

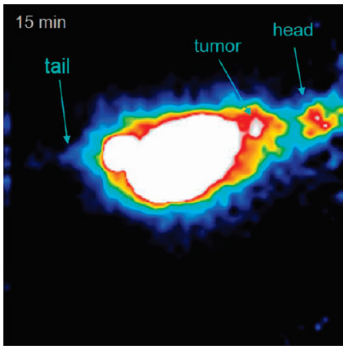

Figure 7. The γ-ray dynamic image of MCF-7 tumor-bearing SCID mouse 15 min after injection of complex **2b**.

and blood (with blood values being 0.62 ± 0.11 %ID/g at 60 min p.i.) while the radioactivity is mainly excreted via the hepatobiliary system. Tumor uptake was 1.04 ± 0.14 %ID/g at 15 min and 0.67 ± 0.06 %ID/g at 60 min leading to a tumor/muscle ratio of 2.2 at 15 min. The corresponding biodistribution data for complex **3b** are presented in Table S3 of the Supporting Information. Complex **3b** displays essentially the same biodistribution behavior as **2b**, showing however a lower tumor uptake of 0.76 ± 0.12 %ID/g at 15 min and 0.36 ± 0.06 %ID/g at 60 min, as well as a lower tumor/muscle ratio of 1.6 at 15 min.

Dynamic γ-Camera Imaging. In scintigraphic imaging performed in SCID mice bearing MCF-7 xenografts with complex **2b**, delineation of the tumor at the left front flank was clear right from the first image obtained at 15 min p.i. (Figure 7 and Supporting Information Figure S6). The total counts of regions of interest (ROIs) corrected for ^{99m}Tc decay are divided by the total counts in mouse and plotted vs time in Figure 8 for the tumor region and its axially symmetric region on the right shoulder serving as background. The percentage of radioactivity in the tumor region is approximately double compared to the background and shows at

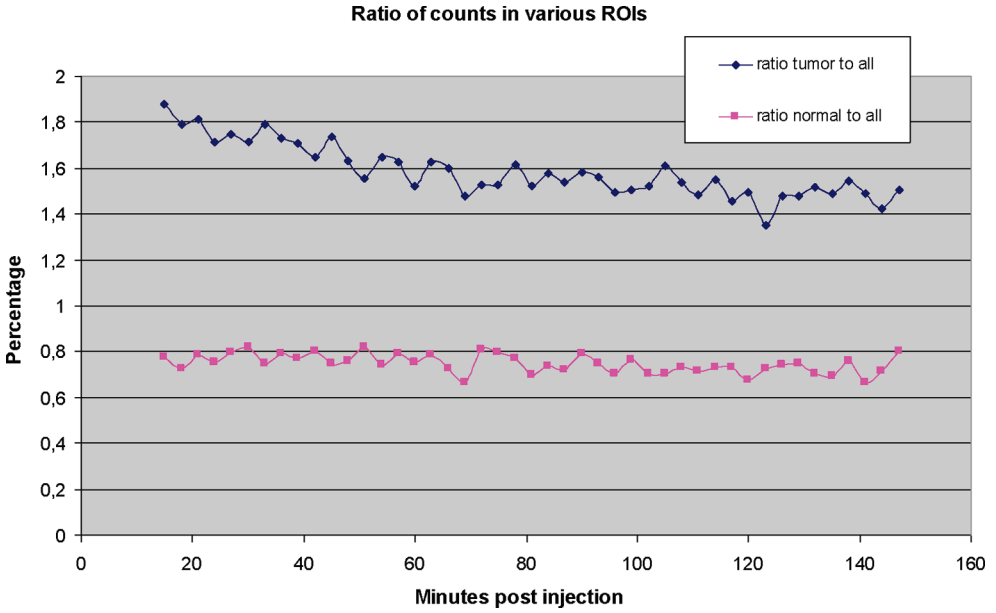

Figure 8. Regions of interest (ROI) plot showing the radioactivity (expressed as percent of total radioactivity measured in the mouse) recorded over time for the tumor region and the axially symmetric region serving as background. Values have been corrected for the decay of ^{99m}Tc.

15 min a 1.9% of total radioactivity in the tumor region dropping to 1.6% at 60 min, in agreement with the behavior of tumor radioactivity in the biodistribution studies.

Discussion

Based on the unique anticancer properties of the 2-(4′-amino)phenylbenzothiazole pharmacophore moiety **1**, the M(I)(CO)$_3$(NNO) complexes **2** and **3** (M = ^{99m}Tc, Re), in which **1** is joined through an amide bond to the metal chelate part, were designed and synthesized aiming at cancer radiodiagnosis and/or radiotherapy. The cell uptake experiments of the Re complexes (performed more extensively for **2a** because of its more intense fluorescence) demonstrated that cell uptake of the complexes by cancer cells approximately corresponds to the sensitivity of these cells to 2-(4′-amino)phenylbenzothiazole derivatives. Specifically, under the fluorescence microscope, complex **2a** displayed clear uptake by the sensitive breast cancer cell lines MCF-7 and T47D, much weaker to no detectable uptake in the less sensitive breast cancer (MDA-231, MDA-468, SKBR-3) and prostate cancer (PC3) cell lines, and no detectable uptake by normal fibroblasts. Apparently, the in vitro selectivity of the 2-(4′-amino)phenylbenzothiazole pharmacophore toward cancer cell lines is still present in the Re complexes. Even though amides of the parent pharmacophore **1**, including the alanyl and lysyl amide prodrugs under clinical evaluation, are known to rapidly and quantitatively revert to the parent amine in the presence of both sensitive and inherently resistant cell lines,[2,5] no conversion of **2a** to its parent amine **1** was detected during its 24 h of incubation with MCF-7 cells, as shown by HPLC analysis (Supporting Information). Therefore, the observed fluorescence can be safely attributed to the intact complex. The selective uptake of the Re complexes by cancer cell lines in combination with their demonstrated stability under the incubation conditions provided the base for the continuation of this work.

Complexes **2a** and **3a** appear to be less cytotoxic than the parent compound **1** and its N-acetylated form based on the IC_{50} values (> 800 nM for **2a** and > 600 nM for **3a**) determined with the MTT assay. Nevertheless, IC_{50} values within the nanomolar to micromolar range indicate that a degree of cytotoxicity is maintained in the complexes. This presents no barrier for the potential radiodiagnostic application of the corresponding ^{99m}Tc complexes because the concentration of ^{99m}Tc formulations in the blood[18] is typically in the picomolar range, orders of magnitude below the IC_{50} values of the complexes, and therefore, their administration presents no cytotoxic danger. For the potential radiotherapeutic applications of **2a** and **3a** with the ^{186}Re and ^{188}Re isotopes the possibility for combined radiotherapy/chemotherapy that would exploit both the cytotoxic properties of the radionuclide and those of the 2-(4′-aminophenyl)benzothiazole emerges as an attractive concept for further exploration.

The parent compound 2-(4′-aminophenyl)benzothiazole (**1**) and other important derivatives bearing 3′-substituents[5,19] have visibly demonstrated by confocal microscopy their ability to enter in the nucleus of MCF-7 cells. In this work, the presence of complex **2a** in the nucleus of MCF-7 cells was examined by fluorescence and confocal microscopy, as its subcellular distribution relates to a potential application of this complex in radiotherapy.[20] To the limit of our optical detection methods, no uptake of **2a** in the nuclei was observed. This finding is in accordance with the lack of conversion of **2a** to the parent amine **1** which, as stated above, has been shown by confocal microscopy to enter the nuclei of MCF-7 cells. According to mechanistic evidence in the literature on the mode of action of anticancer benzothiazoles,[2,19,21] these agents bind to the aryl hydrocarbon receptor (AhR) in the cytosol and the ligand-activated AhR subsequently translocates to the nucleus where transcriptional activation of target genes, such as CYP1A1, takes place. Even though in this work visible translocation of complex **2a** in the nucleus was not observed based on detectable fluorescence, at this point the fate of complex **2a** in the cell is not known and its interaction with the AhR cannot be excluded or supported by our data.

The corresponding ^{99m}Tc complexes **2b** and **3b** were prepared in high yield and high radiochemical purity and were

shown to be stable under a variety of conditions. Uptake experiments revealed higher uptake of both **2b** and **3b** by the MCF-7 and MDA-231 cells compared to the 3T3 mouse fibroblasts used as control. The two complexes displayed comparable entry (with the **3b** being slightly higher), in contrast to the fluorescence results with the Re analogues in which **2b** had a clear advantage, apparently due to its stronger fluorescence (Figure S2). The uptake results with the ^{99m}Tc complexes bring out the exquisite sensitivity of radioactivity as an analytical tool compared to the visibility limitations of optical experiments.

The biodistribution data of complexes **2b** and **3b** in MCF-7 tumor bearing mice were comparable to those observed in healthy mice demonstrating rapid blood and soft tissue clearance, while the radioactivity was mainly excreted via the hepatobiliary system. Tumor uptake was lower for complex **3b** compared to **2b**, despite the presence of the 6-methyl substituent, originally intended to improve metabolic stability[1,3] and to increase lipophilicity and tumor uptake. For **2b**, tumor uptake of 1.04 ± 0.14 %ID/g at 15 min and 0.67 ± 0.06 %ID/g at 60 min is considered satisfactory, leading to a tumor/muscle ratio of 2.2. These values favorably compare to those obtained by others for ^{99m}Tc-labeled agents targeting xenografted MCF-7 tumors in mice. For example, 1.63 ± 0.47 and 1.06 ± 0.53 %ID/g are reported at 30 min for ^{99m}Tc-labeled folate and methotrexate conjugates,[22] 0.45 %ID/g is reported at 30 min for the ^{99m}Tc-labeled derivatized estradiol,[23] 1.15 ± 0.17 %ID/g is reported for D-glucarate, and 0.64 ± 0.07 %ID/g is reported for ^{99m}Tc-sestamibi.[24]

The in vivo planar imaging studies show that after intravenous administration complex **2b** is rapidly cleared from blood circulation (Figure S6) and radioactivity is located in the abdominal region, in accordance with clearance via the hepatobiliary system. The tumor on the left flank region was clearly visualized at the beginning of the dynamic study (15 min p.i., Figure 7), and it remained visible at least up to 120 min. The region of interest (ROI) plot in Figure 8 clearly shows the higher accumulation of radioactivity in the tumor region, while the ratio of the percent of radioactivity in the tumor region (1.9%) over the percent in the symmetrical background region (0.8%) is 2.3 at 15 min, in complete agreement with the biodistribution data. The ROI plot of Figure 8 provides a clean trace of the tumor radioactivity over a 150 min time period, depicting its quick uptake followed by a slow washout.

In order to examine the possibility that the observed uptake is due to increased circulation and/or inflammation around the cancerous tissue, tumor xenograft was developed in SCID mice with PC3 cells that are considered inherently resistant[1,2] to the antitumor benzothiazoles and in our experiments have demonstrated minimal uptake of complex **2a** (Figure S3). The dynamic study performed with complex **2b** (Figure S7) showed no visible accumulation at the tumor, while the corresponding ROI plot reveals slightly higher accumulation in the tumor area with a tumor/muscle ratio of 1.2 at 15 min, compared to corresponding ratio of 2.3 obtained for the MCF-7 tumor bearing mice.

Overall, the experimental findings show that the initial concept for tumor-targeted localization of the ^{99m}Tc radionuclide by the 2-(4′-aminophenyl)benzothiazole pharmacophore moiety is viable and feasible. The design, based on the bifunctional approach, unites the 2-(4′-aminophenyl)benzothiazole with a strong NNO Tc-chelating agent and generates stable complexes that appear to maintain their structure under the standard conditions employed for biological evaluation. The tumor/muscle ratio of 2.3 observed in the imaging studies for the most active of the ^{99m}Tc complexes **2b** is satisfactory and renders this design amenable to further exploration toward the development of specific breast cancer radiopharmaceuticals.

Experimental Section

General. Reagents and solvents were purchased from Aldrich Chemical Co. or Fluka Chemical Co. and used without further purification. $Na^{99m}TcO_4$ was obtained in physiological saline as commercial ^{99}Mo/^{99m}Tc generator eluate (CIS International). Gravity column chromatography was performed on Merck silica gel 60. Elemental analyses for C, H, and N were conducted on a Perkin-Elmer 2400 automatic elemental analyzer. High performance liquid chromatography (HPLC) analysis was performed on a Waters 600E chromatography system coupled to both a Waters 991 photodiode array detector (UV trace for Re complex and ligand) and a GABI γ detector from Raytest (γ trace for ^{99m}Tc). Solvents used in chromatographic analysis were HPLC grade. Separations were achieved on a Macherey-Nagel Nucleosil-100-10-C18 (250 mm × 4.6 mm) column eluted with a binary gradient system at a 1.0 mL/min flow rate. Mobile phase A was 0.1% TFA in methanol, while mobile phase B was 0.1% TFA in water. The elution profile was as follows: 0−1 min 0% A followed by a linear gradient to 75% A in 9 min; this composition was held for another 20 min. After a column wash with 95% A for 5 min the column was re-equilibrated applying the initial conditions (0% A) for 15 min prior to the next injection. IR spectra were recorded as KBr pellets in the range 4000−500 cm^{-1} with a Perkin-Elmer 1600 FT-IR spectrophotometer. Mass spectra were recorded on a ESI Navigator Finnigan spectrometer. UV absorption spectra were obtained on a UV/vis V-560 Jasco spectrophotometer and emission spectra on a PTL-396S Jasco spectrophotometer. NMR spectra were acquired at 25 °C in DMSO-d_6 on a 500 MHz Bruker DRX Avance spectrometer (^{1}H at 500.13 MHz and ^{13}C at 125.77 MHz). Assignment of ^{1}H and ^{13}C NMR chemical shifts was based on two-dimensional correlation experiments (^{1}H−^{1}H COSY, ^{1}H−^{13}C HSQC, ^{1}H−^{13}C HMBC, and ^{1}H−^{1}H NOESY) recorded using standard pulse sequences. The chemical shifts for ^{1}H and ^{13}C are reported in ppm (δ) relative to tetramethylsilane (TMS). Fluorescence microscope images were obtained with a Nicon E400 microscope equipped with digital camera JVC, TK-C1381. Confocal images were obtained with a Leica confocal laser scanning microscope (TCS SP5, DMI6000, inverted, with the acquisition software LAS-AF, at 23−24 °C) equipped with a _63 NA 1.4 objective. All tested compounds were > 95% pure as determined by HPLC and C, H, N elemental analysis and confirmed by NMR spectroscopy.

Synthesis. The preparation of complex **2a** and its complete characterization, as well as the preparation of complex **2b**, have been described in detail in our previous communication.[10]

2-(4′-Aminophenyl)-6-methylbenzothiazole (4). The preparation of 6-methyl-2-aminothiophenol[3] (**6**) which is not commercially available, is described first. A mixture of 2-amino-6-methylbenzothiazole (**7**, 12.5 g, 76 mmol) in aqueous NaOH (10 M, 100 mL) was stirred under reflux overnight, under a constant nitrogen atmosphere, after it was properly degassed. The reaction mixture was poured into ice−water (150 mL), acidified with concentrated HCl to pH 2−3, neutralized with K_2CO_3, and extracted with toluene. The organic phase was washed with water and dried over Na_2SO_4, and the solvent was removed under vacuum. The residue was recrystallized from methanol, yielding yellow-brown crystals of compound **6**.[13] Yield 90%. For the preparation of **4**, a mixture of aminothiophenol **6** (1.39 g, 10 mmol) and 4-aminobenzoic acid (1.37 g, 10 mmol) in polyphosphoric acid (20 g) was heated at 220 °C for 4 h. After cooling, the reaction mixture was poured into ice-cold

aqueous sodium carbonate (10% w/v) and stirred until gas evolution ceased. The precipitated product was collected by filtration under vacuum, washed with water, and crystallized from MeOH/H_2O to afford **4** as a brown powder. Yield: 56%. Mp: 191−196 °C. ^{1}H and ^{13}C data for both **6** and **4** are provided in Table S1.

***N*-(4′-Benzothiazol-2-yl-phenyl)-2-chloroacetamide (9).** Chloroacetyl chloride (438 mg, 3.9 mmol, 1.2 equiv) was added dropwise and under nitrogen to a stirred solution of **4** (760 mg, 3.2 mmol) and triethylamine (543 mg, 5.4 mmol, 1.7 equiv) in 5 mL of anhydrous CH_2Cl_2, at 0 °C. The reaction mixture was stirred for 30 min at 0 °C and then for 1 h at ambient temperature under nitrogen, and the solution turned gradually cloudy because of precipitation of the product. Compound **9** was collected as a yellowish powder after filtration and washings with a minimum amount of dichloromethane, water (2 × 10 mL), and saturated aqueous sodium bicarbonate (2 × 10 mL) followed by air drying. Yield: 75%. ^{1}H and ^{13}C data for **9** are provided in Table S1. Anal. Calcd for $C_{16}H_{13}ClN_2OS$: C, 60.66; H, 4.14; N, 8.84. Found: C, 59.89; H, 3.96; N, 9.11.

***N*-(Pyridine-2-ylmethyl)-*N*-[4′-(benzothiazol-2-yl)-(phenylaminoacetyl)]aminoacetic Ethyl Ester (11).** A solution of *N*-(2-pyridylmethyl)aminoacetic acid ethyl ester (214 mg, 1.1 mmol) prepared as previously described[14] in 2 mL of acetonitrile was added to a stirred solution of **9** (317 mg, 1 mmol) and diisopropylethylamine (194 mg, 1.5 mmol) in 7 mL of acetonitrile. The reaction mixture was stirred for 18 h under reflux and then evaporated under vacuum. The residue was dissolved in CH_2Cl_2 (15 mL), washed with distilled water (2 × 10 mL), dried over Na_2SO_4, and evaporated under vacuum to give a brown solid. Purification by silica gel column chromatography with ether as eluent solvent afforded **11** as a white solid. Yield: 52%. ^{1}H and ^{13}C data for **11** are provided in Table S1. Anal. Calcd for $C_{25}H_{24}N_4O_3S$: C, 65.20; H, 5.25; N, 12.17. Found: C, 65.34; H, 5.39; N, 12.38.

Re Complex 3a. To a solution of **11** (47 mg, 0.1 mmol) in 5 mL of acetonitrile was added 2 mL of aqueous solution of NaOH (4 mg, 0.1 mmol), and the mixture was stirred for 15 min at 70 °C. A 5 mL solution of the precursor $[NEt_4]_2[fac\text{-}Re(CO)_3(Br)_3]$ (77 mg, 0.1 mmol) in acetonitrile was subsequently added and the mixture was stirred under reflux for 3 h to afford **3a** as a white precipitate. Yield: 84%. IR (KBr, cm^{-1}): 2016, 1918, 1869. ^{1}H and ^{13}C data are provided in Table S1. MS (ESI): m/z $(M + H)^+$ 717.19 and 715.14 (calculated for $C_{27}H_{21}N_4O_6{}^{185}ReS$ and $C_{26}H_{20}N_4O_6S{}^{187}Re$, 717.08 and 715.07, respectively). Anal. Calcd for $C_{27}H_{21}N_4O_6ReS$: C, 45.31; H, 2.96; N, 7.83. Found: C, 45.25; H, 2.91; N, 7.89.

Synthesis of ^{99m}Tc Complex 3b. An amount of 400 μL of a freshly prepared solution of the *fac*-$[^{99\ m}Tc(CO)_3(H_2O)_3]^+$ precursor[3] (pH 7.5) was added to a vial containing a 100 μL solution of **11** (10^{-3} M) in acetonitrile. Prior basic hydrolysis of the ester group of **11** was not necessary in this case. The vial was sealed, flushed with N_2, and heated for 30 min at 75 °C. HPLC analysis demonstrated the formation of a single complex (radiochemical yield of >90%) which is stable for at least 6 h, as evidenced by HPLC. The radioactivity recovery of the HPLC column after the injection of **3b** was monitored and found to be quantitative. The identity of the complex was established by comparative HPLC analysis (Figure S1) using a sample of the well-characterized complex **3a** as reference.

Cell Uptake and MTT Colorimetric Assay Experiments for the Re Complexes 2a and 3a . These experiments are described in the Supporting Information.

Nuclear Uptake Study of Re Complex 2a. About 10^6 cells in D-MEM growth medium (PAA Laboratories), supplemented with 10% FBS (PAA Laboratories), 100 U/mL penicillin (PAA Laboratories), and 100 μg/mL streptomycin (PAA Laboratories), were seeded for attachment on sterilized coverslips in six-well plates for 24 h in a 5% CO_2 incubator at 37 °C. The day after seeding, cells were incubated in the presence of 80 μM complex **2a**. The cells were washed and harvested by replacing the growth medium with trypsin/EDTA solution (PAA Laboratories), incubating the culture for 5 min in a 5% CO_2 incubator at 37 °C, and centrifuging (800g × 10 min). The cell pellet was suspended in 2 mL of a hypotonic KCl solution (75 mM), incubated for 10 min at room temperature, and centrifuged (800g × 10 min). Subsequently, the cell nuclei enriched preparation was fixed in 2 mL of a methanol/acetic acid solution (3:1) as fixative. The fixation procedure was repeated twice, and the final precipitate was suspended in 0.5 mL of methanol/acetic acid solution (3:1). An amount of 50 μL of the suspension was spread on a microscope slide, air-dried, mounted with an antifade solution of *p*-phenylenediamine (PPD, Sigma), and observed with a fluorescence microscope (Nicon E400 equipped with digital camera JVC, TK-C1381). The antifade solution of PPD was prepared by dissolving 10 mg of PPD in 1 mL of PBS buffer and 9 mL of glycerol and adjusting the pH to 8 with carbonate−bicarbonate buffer (0.5 M).

Cell Uptake of ^{99m}Tc Complexes 2b and 3b. Cells (MCF-7, MDA-231, 3T3, 5 × 10^5/mL) were seeded in a 24-well plate and allowed to adhere for a 24 h period before they were treated with 50 μL solutions of the $^{99\ m}$Tc complexes (0.2 μCi/mL) followed by incubation for 1, 3, and 5 h. The supernatant was removed and kept separately, while the cells were washed with PBS (2 × 0.5 mL), combining the washings with the separated supernatant. The cells were finally lysed by means of 1 N NaOH solution (2 × 0.5 mL). These lysates were placed separately before radioactivity was measured. The percent radioactivity uptake was calculated using the formula % radioactivity uptake = 100(lysate counts)/(cell washing counts + supernatant counts). The result for each time interval was the mean value of four wells, and each experiment was repeated three times.

Biodistribution of 2b and 3b in Mice Bearing MCF-7 Xenografts. Athymic SCID mice (female, 6−8 week old, 17−20 g) were obtained from the breeding facilities of the Institute of Biology, NCSR "Demokritos". For xenograft development, a bolus containing a suspension of (3−5) × 10^6 freshly harvested human MCF-7 breast cancer cells and NIH 3T3 mouse fibroblasts (ratio MCF7/3T3 = 3:1) in serum-free DMEM was incoculated subcutaneously into the left flank of each mouse. The inclusion of 3T3 cells was performed because it has been demonstrated that it facilitates xenograft development.[25] Care was exercised to develop the tumor at a site away from the liver to allow for clear depiction of the radioactivity accumulation.

The animals were kept under aseptic conditions and were observed daily for tumor development. Mice were used as soon as tumors became palpable (100−150 mg), which was in approximately 2−3 weeks.

For the biodistribution study, 0.1 mL containing 2 μCi of complex **2b** or **3b** in PBS buffer, pH 7.4, was injected through the tail vein of each xenograft-bearing mouse. Animals were sacrificed in groups of five at 15 and 60 min by ether anesthesia. Tissues and organs of interest were immediately collected, weighed, and measured for radioactivity in a NaI well γ-counter (Canberra Packard Auto-Gamma 5000 series). Stomach and intestines were not emptied of their contents but used as collected. Biodistribution data were calculated as percent injected dose per gram of tissue (%ID/g) using an in-house computer program and employing appropriate standards; they are expressed as the mean of values ± standard deviation (mean ± SD).

In vivo studies were performed in compliance with European legislation. The Hellenic authorities approved all animal protocols.

Dynamic Imaging Studies in MCF-7 Xenograft-Bearing Mice. MCF-7 tumors were developed as described in the previous paragraph. An amount of 0.1 mL (200−300 μCi) of **2b** was injected intravenously into the tail vein of each mouse. Mice were anesthetized by the subcutaneous injection of 1.0 g of 2,2,2-tribromomethanol in 1.0 mL of 2-methyl-2-butanol at a dose of 300 μL per 30 g of body weight. They were subsequently transferred at the imaging lab and placed on the camera bed

at approximately 10 min after tracer's injection. The imaging experiment was performed four times with comparable results.

The camera used was a dedicated, high resolution, and high sensitivity "small animal imaging system based on position sensitive photomultiplier tubes and a NaI(Tl) pixelized scintillator" described in detail elsewhere.[26] The typical position for planar studies minimizes the distance between the mouse and the collimator. Thus, a resolution of 1.5 mm is achieved and sequential acquisition of 2 min images is possible. The images were stored in raw format and processed with ImageJ software.

Regions of interest (ROIs) were drawn in the tumor region and on a background region (right shoulder). The total counts were corrected for ^{99m}Tc decay, and they were plotted as a function of time (acquisition frame number). Normally ROI analysis was carried out in SPECT mode; however, in this case, the lack of other organs in the shoulder region and the symmetry of the two shoulders gave a satisfactory approximation of radiopharmaceutical concentration as a function of time. The total counts in the ROI are divided by the number of total counts in the mouse; this provides the percentage of radioactivity in each ROI, which is comparable to biodistribution results.

Acknowledgment. M.P. gratefully acknowledges financial support by ASPIS Bank, Greece. The authors thank Dr. D. Vourloumis of the Institute of Physical Chemistry of NCSR "Demokritos" for providing the MCF-7 breast cancer cells, as well as Dr. D. Kletsas and Dr. H. Pratsinis of the Institute of Biology of NCSR "Demokritos" for providing the MILA fibroblasts. The authors also thank Dr. K. Stamatakis of the Institute of Biology of NCSR "Demokritos" for obtaining the fluorescence spectra of Figure S2.

Supporting Information Available: Experimental procedure for cell uptake experiments; MTT colorimetric assay and stability studies for complexes **2** and **3**; ^{1}H and ^{13}C NMR data for compounds **4**, **6**, **9**, **11**, **3a**; biodistribution data for complex **3b** in healthy mice; biodistribution data for complex **3b** in SCID mice bearing MCF-7 xenografts; comparative HPLC chromatograms for complexes **3a** and **3b**; fluorescence spectra of ligands **10** and **11**; images of the uptake of complex **2a** by different cancer lines; images of the uptake of complex **2a** by cancer lines at different concentrations; MTT assay curves for complexes **2a** and **3a**; dynamic imaging study of complex **2b** in MCF-7 tumor bearing mouse; dynamic image of complex **2b** in PC3 tumor bearing mouse and corresponding ROI graph. This material is available free of charge via the Internet at http://pubs.acs.org.

References

(1) Bradshaw, T. D.; Stevens, M. F. G.; Westwell, A. D. The discovery of the potent and selective antitumor agent 2-(4-amino-3-methylphenyl)benzothiazole (DF 203) and related compounds. *Curr. Med. Chem.* **2001**, *8*, 203–210.

(2) Bradshaw, T. D.; Westwell, A. D. The development of the antitumour benzothiazole prodrug, Phortress, as a clinical candidate. *Curr. Med. Chem.* **2004**, *11*, 1241–1253.

(3) Shi, D.-F.; Bradshaw, T. D.; Wrigley, S.; McCall, C. J.; Lelieveld, P.; Fichtner, I.; Stevens, M. F. G. Antitumor benzothiazoles. 3. Synthesis of 2-(4-aminophenyl)benzothiazoles and evaluation of their activities against breast cancer cell lines in vitro and in vivo. *J. Med. Chem.* **1996**, *39*, 3375–3384.

(4) Bradshaw, T. D.; Wrigley, S.; Shi, D.-F.; Schultz, R. J.; Paull, K. D.; Stevens, M. F. G. 2-(4-Aminophenyl)benzothiazoles: novel agents with selective profiles of in vitro and in vivo activity. *Br. J. Cancer* **1998**, *77*, 745–752.

(5) Chua, M.-S.; Shi, D.-F.; Wrigley, S.; Bradshaw, T. D.; Hutchinson, I.; Shaw, P. N.; Barrett, D. A.; Stanley, L. A.; Stevens, M. F. G. Antitumor benzothiazoles. 7. Synthesis of 2-(4-acylaminophenyl)-benzothiazoles and investigations into the role of acetylation in the antitumor activities of the parent amines. *J. Med. Chem.* **1999**, *42*, 381–392.

(6) Kashiyama, E.; Hutchinson, I.; Chua, M.-S.; Stinson, S. F.; Phillips, L. R.; Kaur, G.; Sausville, E. A.; Bradshaw, T. D.; Westwell, A. D.; Stevens, M. F. G. Antitumor benzothiazoles. 8. Synthesis, metabolic formation, and biological properties of the C- and N-oxidation products of antitumor 2-(4-aminophenyl)-benzothiazoles. *J. Med. Chem.* **1999**, *42*, 4172–4184.

(7) Bradshaw, T. D.; Shi, D.-F.; Schultz, R. J.; Paull, K. D.; Kelland, L.; Wilson, A.; Garner, C.; Fiebig, H. H.; Wrigley, S.; Stevens, M. F. G. Influence of 2-(4-aminophenyl) benzothiazoles on growth of human ovarian carcinoma cells in vitro and in vivo. *Br. J. Cancer* **1998**, *78*, 421–429.

(8) (a) Hutchinson, I.; Chua, M.-S.; Browne, H. L.; Trapani, V.; Bradshaw, T. D.; Westwell, A. D.; Stevens, M. F. G. Antitumor benzothiazoles. 14. The synthesis and in vitro biological properties of fluorinated 2-(4-aminophenyl)benzothiazoles. *J. Med. Chem.* **2001**, *44*, 1446–1455. (b) Hutchinson, I.; Jennings, S. A.; Vishnuvajjala, B. R.; Westwell, A. D.; Stevens, M. F. G. Antitumor benzothiazoles. 16. Synthesis and pharmaceutical properties of antitumor 2-(4-aminophenyl)-benzothiazole amino acid prodrugs. *J. Med. Chem.* **2002**, *45*, 744–747.

(9) (a) Liu, S. The role of coordination chemistry in the development of target-specific radiopharmaceuticals. *Chem. Soc. Rev.* **2004**, *33*, 445–461. (b) Liu, S. Bifunctional coupling agents for radiolabelling of biomolecules and target-specific delivery of metallic radionuclides. *Adv. Drug Delivery Rev.* **2008**, *60*, 1347–1370.

(10) Tzanopoulou, S.; Pirmettis, I. C.; Patsis, G.; Paravatou-Petsotas, M.; Livaniou, E.; Papadopoulos, M.; Pelecanou, M. Synthesis, characterization, and biological evaluation of M(I)(CO)3(NNO) complexes (M = Re, ^{99m}Tc) conjugated to 2-(4-aminophenyl)-benzothiazole as potential breast cancer radiopharmaceuticals. *J. Med. Chem.* **2006**, *49*, 5408–5410.

(11) (a) Arano, Y. Recent advances in ^{99m}Tc radiopharmaceuticals. *Ann. Nucl. Med.* **2002**, *16*, 79–93. (b) Mindt, T.; Struthers, H.; Garcia-Garayoa, E.; Desbouis, D.; Schibli, R Strategies for the development of novel tumor targeting technetium and rhenium radiopharmaceuticals. *Chimia* **2007**, *61*, 725–731. (c) Lambert, B.; de Klerk, J. M. H. Clinical applications of ^{188}Re-labelled radiopharmaceuticals for radionuclide therapy. *Nucl. Med. Commun.* **2006**, *27*, 223–229. (d) Hashimoto, K.; Yoshihara, K. Rhenium complexes labeled with Re-186, Re-188 for nuclear medicine. *Technetium Rhenium Top. Curr. Chem.* **1996**, *176*, 275–291.

(12) (a) Deutsch, E.; Libson, K.; Vanderheyden, J.-L.; Ketring, A. R.; Maxon, H. R. The chemistry of rhenium and technetium as related to the use of isotopes of these elements in therapeutic and diagnostic nuclear-medicine. *Nucl. Med. Biol.* **1986**, *13*, 465–477. (b) Dilworth, J.; Parrot, S. The biomedical chemistry of technetium and rhenium. *Chem. Soc. Rev.* **1998**, *27*, 43–55.

(13) Phoon, C. W.; Ng, P. Y.; Ting, A. E.; Yeo, S. L.; Sim, M. M. Biological evaluation of hepatitis C virus helicase inhibitors. *Bioorg. Med. Chem. Lett.* **2001**, *11*, 1647–1650.

(14) Inoue, H.; Konda, M.; Hashiyama, T.; Otsuka, H.; Watanabe, A.; Gaino, M.; Takahashi, K.; Date, T.; Okamura, K.; Takeda, M.; Narita, H.; Murata, S.; Odawara, A.; Sasaki, H.; Nagao, T. Synthesis and biological evaluation of alkyl, alkoxy, alkylthio, or amino-substituted 2,3-dihydro-1,5-benzothiazepin-4(5*H*)-ones. *Chem. Pharm. Bull.* **1997**, *45* (6), 1008–1026.

(15) Policar, C.; Lambert, F.; Cesario, M.; Morgenstern-Badarau, I. An inorganic helix $[Mn(IPG)(MeOH)]_n[PF6]_n$: structural and magnetic properties of a syn−anti carboxylate-bridged manganese(II) chain involving a tetradentate ligand. *Eur. J. Inorg. Chem.* **1999**, *12*, 2201–2207.

(16) Alberto, R.; Egli, A.; Abram, U.; Hegetschweiler, K.; Gramlich, V.; Schubiger, P. A. Synthesis and reactivity of $[NEt_4]_2[ReBr_3(CO)_3]$. Formation and structural characterization of the clusters $[NEt_4][Re_3(\mu\text{-}3\text{-}OH)(\mu\text{-}OH)_3(CO)_9]$ and $[NEt_4][Re_2(\mu\text{-}OH)_3(CO)_6]$ by alkaline titration. *J. Chem. Soc., Dalton Trans.* **1994**, *19*, 2815–2820.

(17) Alberto, R.; Schibli, R.; Egli, A.; Schubiger, A. P.; Abram, U.; Kaden, T. A. A novel organometallic aqua complex of technetium for the labeling of biomolecules: synthesis of $[^{99m}Tc(OH_2)_3(CO)_3]^+$ from $[^{99m}TcO_4]^-$ in aqueous solution and its reaction with a bifunctional ligand. *J. Am. Chem. Soc.* **1998**, *120*, 7987–7988.

(18) Hill, D. M.; Barnes, R. K.; Wong, H. K. Y.; Zawadzki, A. W. The quantification of technetium in generator-derived pertechnetate using ICP-MS. *Appl. Radiat. Isot.* **2000**, *53*, 415–419.

(19) Bradshaw, T. D.; Stone, E. L.; Trapani, V.; Leong, C.-O.; Matthews, C. S.; te Poele, R.; Stevens, M. F. G. Mechanisms of aquired resistance to 2-(4-amino-3-methylphenyl)benzothiazole in breast cancer lines. *Breast Cancer Res. Treat.* **2008**, *110*, 57–68.

(20) (a) Kassis, A. I.; Adelstein, S. J. Radiobiologic principles in radionuclide therapy. *J. Nucl. Med.* **2005**, *46* (Suppl.), 4S–12S. (b) Goddu, S. M.; Howell, R. W.; Rao, D. V. Cellular dosimetry: absorbed fractions for monoenergetic electron and alpha particle sources and S-values for radionuclides uniformly distributed in different cell compartments. *J. Nucl. Med.* **1994**, *35*, 303–316.

(21) (a) Bradshaw, T. D.; Fichtner, I.; Bibby, M. J.; Double, J. A.; Cooper, P. A.; Alley, M. C.; Tomaszewjski, J. E.; Donahue, S.; Stinson, S. F.; Sausville, E. A.; Stevens, M. F. G. Preclinical evaluation of amino acid prodrugs of novel antitumor 2-(4-aminomethylphenyl)benzothiazoles. *Mol. Cancer Ther.* **2002**, *1*, 239–246. (b) Loaiza-Pérez, A. I.; Trapani, V.; Hose, C.; Singh, S. S.; Trepel, J. B.; Stevens, M. F. G.; Bradshaw, T. D.; Sausville, E. A. Aryl hydrocarbon receptor mediates sensitivity of MCF-7 breast cancer cells to antitumor agent 2-(4-amino-3-methylphenyl)benzothiazole. *Mol. Pharmacol.* **2002**, *61*, 13–19.

(22) Okarvi, S. M.; Jammaz, I. A. Preparation and in vitro and in vivo evaluation of technetium-99m-labeled folate and methotrexate conjugates as tumor imaging agents. *Cancer Biother. Radiopharm.* **2006**, *21*, 49–60.

(23) Takahashi, N.; Yang, D. J.; Kohanim, S.; Oh, Ch.-S.; Yu, D.-F.; Azhdarinia, A.; Kurihara, H.; Zhang, X.; Chang, J. Y.; Kim, E. E. Targeted functional imaging of estrogen receptors with ^{99m}Tc-GAP-EDL. *Eur. J. Nucl. Med. Mol. Imaging* **2007**, *34*, 354–362.

(24) Liu, Z.; Stevenson, G. D.; Barrett, H. H.; Kastis, G. A.; Bettan, M.; Furenlid, L. R.; Wilson, D. W.; Woolfenden, J. M.; Pak, K. Y. ^{99m}Tc glucarate high-resolution imaging of drug sensitive and drug resistant human breast cancer xenografts in SCID mice. *Nucl. Med. Commun.* **2004**, *25*, 711–720.

(25) Tuxhorn, J. A.; McAlhany, S. J.; Dang, T. D.; Ayala, G. E.; Rowley, D. R. Stromal cells promote angiogenesis and growth of human prostate tumors in a differential reactive stroma (DRS) xenograft model. *Cancer Res.* **2002**, *62*, 3298–3307.

(26) Loudos, G.; Majewski, S.; Wojcik, R.; Weisenberger, A.; Sakellios, N.; Nikita, K.; Uzunoglu, N.; Bouziotis, P.; Xanthopoulos, S.; Varvarigou, A. Performance evaluation of a dedicated camera suitable for dynamic radiopharmaceuticals evaluation in small animals. *IEEE Trans. Nucl. Sci.* **2007**, *54*, 454–460.